



## Full length article

# CoFe<sub>2</sub>O<sub>4</sub> coated carbon fiber paper fabricated via a spray pyrolysis method for trapping lithium polysulfide in Li-S batteries

Xiaohua Feng<sup>a,\*</sup>, Qian Wang<sup>b</sup>, Rongrong Li<sup>a</sup>, Hua Li<sup>a,\*</sup>

<sup>a</sup> Ningbo Institute of Materials Technology and Engineering, Chinese Academy of Sciences, No. 1219 Zhongguan West Road Zhenhai District, Ningbo 315201, China

<sup>b</sup> School of Chemistry and Chemical Engineering, Harbin Institute of Technology, No. 92 West-Da Zhi Street, Harbin 150001, China



## ARTICLE INFO

## Keywords:

CoFe<sub>2</sub>O<sub>4</sub> coating  
Carbon fiber  
Shuttling effect  
Li-S batteries  
Battery performances

## ABSTRACT

Here we report the construction of CoFe<sub>2</sub>O<sub>4</sub> coating on carbon fiber and the coated paper was used as the interlayer between the separator and cathode of Li-S batteries. The amorphous CoFe<sub>2</sub>O<sub>4</sub> coating was deposited by the industry-oriented spray pyrolysis technique and carbon fiber was completely wrapped by the coating. Compared to the non-coated carbon fiber, the coated carbon fiber as the interlayer exhibits a superior reversible capacity of 1086 mA h g<sup>-1</sup> at moderate current of 0.1C and a low decay rate in the capacity of 0.043% per cycle after 1000 cycles at 1C. Excellent long-term cycling life and rate capacity were also achieved through the coated interlayer. The specially designed interlayer showed remarkable capability to trap effectively the intermediate LPS (lithium polysulfide). The significantly inhibited “shuttle effect” of LPS would give insight into designing and making the interlayer by using new coating materials for enhanced performances of the Li-S batteries.

## 1. Introduction

Compared to the commercial batteries, Li-S batteries have high theoretical energy density of 2600 Wh·kg<sup>-1</sup>, high theoretical specific capacity of 1675 mAh·g<sup>-1</sup>, and the natural abundance, environmental friendliness and low cost of sulfur [1]. Li-S batteries would therefore be a strong candidate for the next generation of batteries to meet the increasing energy storage demand of electronics products. However, incomplete active S utilization, poor Coulombic efficiency, and fast capacity degradation persist as the major concerns for the batteries for potential commercial applications [2]. It has been clarified that these drawbacks are related to low electrical conductivity of sulfur and its discharge products (Li<sub>2</sub>S<sub>2</sub>/Li<sub>2</sub>S) [3], large volume change of electrode and dissolution of LPS species [4]. Encapsulating or filling S into conductive and porous matrix materials [5], reserving space for the volume expansion of active materials [6] and constructing adsorption barrier layer of LPS [7] are likely the most effective strategy to improve electrochemical performance of Li-S batteries.

For the Li-S cells, the redox reaction involves dissolution of the intermediate LPS into organic electrolyte and further migration within the electrolyte, which drives the “shuttle effect” and causes loss of active S [8], in turn triggering increased electrolytic viscosity, enhanced lithium anode surface passivation and formation of an unstable solid-electrolyte interphase [9,10]. The ultimate consequences are

performance decay of the batteries in terms of deteriorated cycle stability and high-rate capacity. It is therefore essential to immobilize the dissolved intermediates LPS for Li-S batteries during operation. To date, a variety of techniques have been attempted to tackle the LPS issue. Among the effective ways, encapsulating sulfur into nanostructured carbon [5,11] or its modified derivatives [12] is claimed promising in stabilizing the LPS and electrolyte within the cathode region. Addition of a modified interlayer between the cathode and the separator is also found useful to inhibit and even trap the LPS [13]. It is reported that a simple adjustment of Li-S battery configuration by placing a bifunctional microporous carbon paper in between cathode and separator can improve the active material utilization and capacity retention [14]. The insertion of the microporous carbon interlayer decreases the internal charge transfer resistance and localizes the soluble LPS species [14]. The extra layer like various carbonaceous materials could act as physical spatial obstacles suppressing effectively the spreading of LPS [15,16], yet delaying the transfer rate of Li<sup>+</sup>. Carbonaceous materials usually demonstrate substantial capacity improvement over the first a few hundred cycles, but they suffer significant decay upon long term cycling due to the weak interaction between LPS and carbon [17]. Therefore, chemical adsorption and chemical interaction must be taken into account for capturing the LPS by forming chemical bonds between metal oxide and LPS. A series of metal oxides such as TiO<sub>2</sub> [18], SnO<sub>2</sub> [19], ZnO [20], MnO<sub>2</sub> [21], V<sub>2</sub>O<sub>5</sub> [22], CuO, Co<sub>3</sub>O<sub>4</sub>, Fe<sub>2</sub>O<sub>3</sub> and their

\* Corresponding author.

E-mail addresses: [xhfeng@nimte.ac.cn](mailto:xhfeng@nimte.ac.cn) (X. Feng), [lihua@nimte.ac.cn](mailto:lihua@nimte.ac.cn) (H. Li).

<https://doi.org/10.1016/j.apsusc.2019.01.145>

Received 24 December 2018; Accepted 21 January 2019

Available online 23 January 2019

0169-4332/ © 2019 Published by Elsevier B.V.

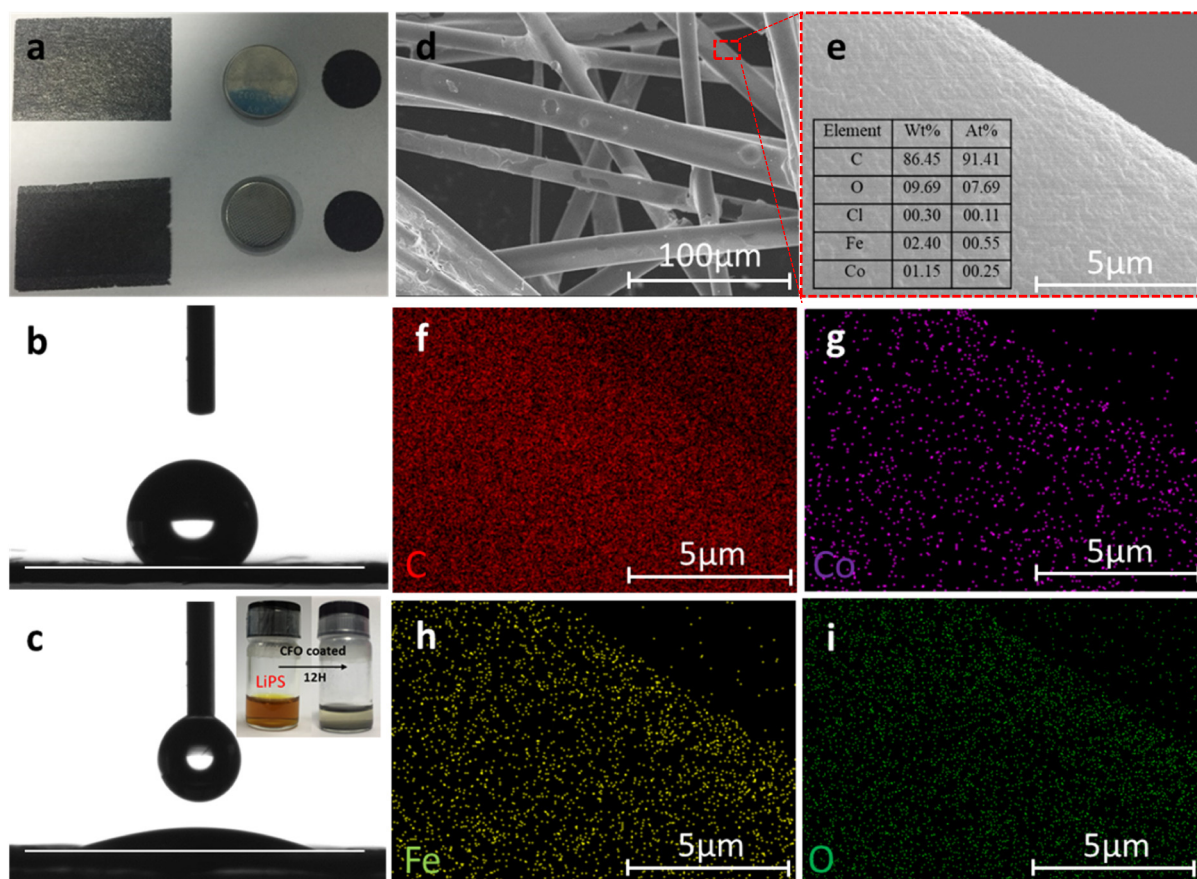


**Fig. 1.** (a) Photograph of the uncoated (top) and CFO coated carbon fiber (bottom), 16 mm disk, (b) Surface wetting of the water droplet on the carbon fiber and (c) CFO coated carbon fiber, the inset image is visualization photos of LPS adsorption by CFO coated carbon fiber in DOL/DME solution for 12 h. (d) SEM image and EDS element mapping of (e) position, the inset table is element ratio in the CFO coated carbon fiber (f) carbon, (g) cobalt, (h) iron, (i) oxygen.

low state oxides [23–26] with multiple specified structures have been used to confine LPS. Elongated cycling life and specific capacities have been reported. Apart from the mono metal oxides, polymetallic oxides containing two different metal ions also exhibited exciting electrochemical activities [27]. Iron-based spinel  $\text{CoFe}_2\text{O}_4$  (CFO) one of the oxides that are competitive in semiconducting properties, chemical constancy, mechanical inflexibility, natural abundance, and eco-friendliness [28–32]. It is anticipated that the polar/hydrophilic nature of CFO favors its strong chemical bonding with LPS and in turn confines its diffusion.

Spray pyrolysis is a well-established technique for depositing metal oxides such as ZnO [17],  $\text{TiO}_2$  [33,34],  $\text{Fe}_2\text{O}_3$  [35], CuO [36],  $\text{SnO}_2$  [37],  $\text{Fe}_2(\text{MoO}_4)_3$  [38] etc. Taking into account the cost efficiency and ease of large-scale thin film fabrication [39], glass substrate is usually employed for relevant investigation. Thermal decomposition temperature of most oxide precursors lies in the range of 100–300 °C, below the oxidation temperature of carbon fiber. In this work, carbon fiber was used as substrate for CFO coating deposition. The CFO coating showed excellent electrical conductivity, complex physical space framework and good wettability. Combination of carbon fiber and CFO coating provided a dual-block confined interlayer structure, facilitating the transport of electrons, spatial obstacle of polysulfide and chemical adsorption dissolved LPS during the discharging process. Significantly increased capacity, enhanced long-term cycling stability and rate capability along with a lowered voltage barrier have been achieved.

## 2. Materials and methods

### 2.1. Preparation of CFO coated carbon fiber

Prior to the coating deposition, the carbon fiber substrates were cleaned in turn with hydrochloric acid and distilled water. The precursor solution was prepared by mixing ferric nitrate  $\text{Fe}(\text{NO}_3)_3 \cdot 9\text{H}_2\text{O}$  and cobalt nitrate  $\text{CoCl}_2 \cdot 6\text{H}_2\text{O}$  in double distilled water with the molar ratio of 2:1. The solution was freshly prepared to avoid recrystallization of the starting materials that may block the spray pyrolysis nozzle before spraying. The CFO coatings were deposited on the pretreated carbon fiber substrate (5.0 cm × 3.0 cm) using the spray pyrolysis technique. To obtain homogeneous, well crystallized and reproducible CFO coatings, spray parameters were optimized. The key parameters, substrate temperature (400 °C), spray rate (1 ml/min), distance between substrate and nozzle (30 cm), nozzle diameter (0.3 mm), and pressure of the compressed air (2 bar) were selected and kept constant during the spraying. The basic reaction for formation of the CFO coatings was given by [40]:  $\text{CoCl}_2 \cdot 6\text{H}_2\text{O} + 2\text{Fe}(\text{NO}_3)_2 \cdot 9\text{H}_2\text{O} \rightarrow \text{CoFe}_2\text{O}_4 + 2\text{HCl} \uparrow + 23\text{H}_2\text{O} \uparrow + 4\text{NO}_2 \uparrow + 1/2\text{O}_2 \uparrow$ .

After the coating deposition, the CFO coated samples were laminated into 16 mm diameter disk for assembling the battery.

### 2.2. Cell assembly

Sulfur cathode slurry was prepared by mixing 50 wt% of sulfur powder, 40 wt% of carbon black (Super P) and 10 wt% of polyvinylidene fluoride (PVDF) binder in an *N*-methylpyrrolidinone (BMP) solution and stayed overnight. The slurry was tape-casted onto carbon

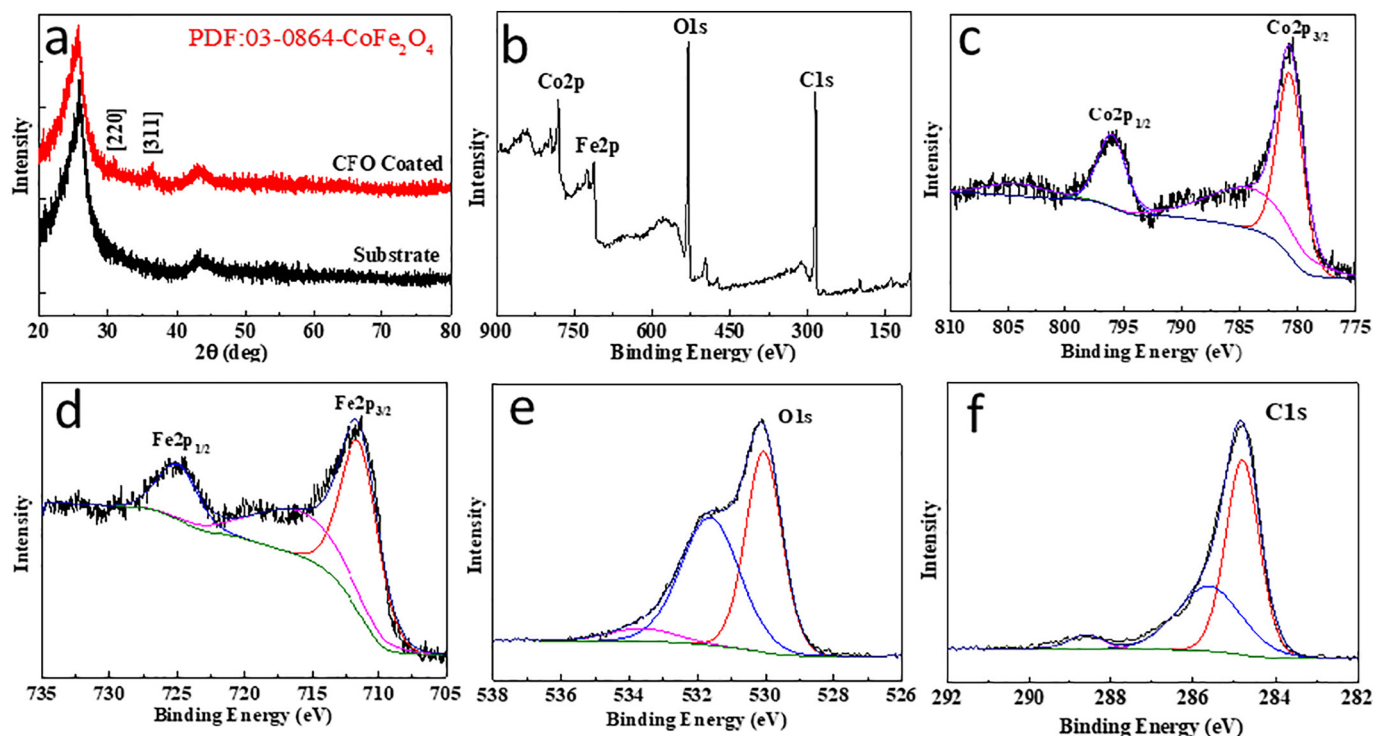


Fig. 2. (a) XRD spectra and XPS spectra of CFO coated carbon fiber (b) wide scan, (c) Co2p, (d) Fe2p, (e) O1s and (f) C1s.

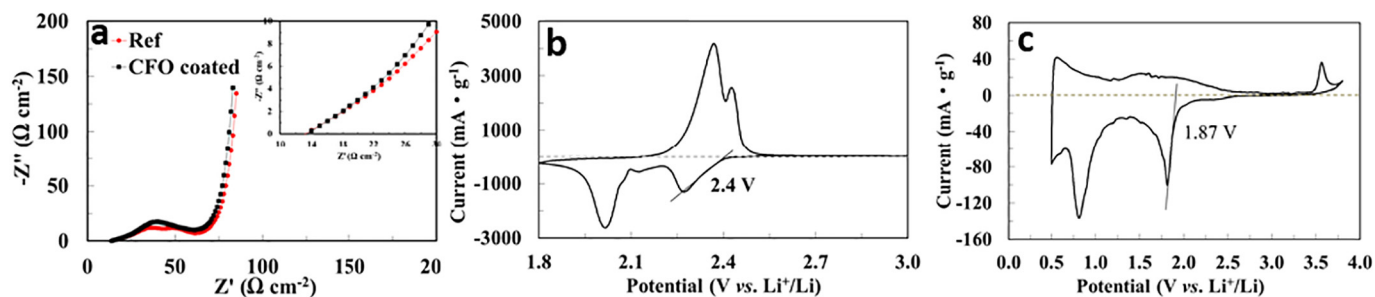


Fig. 3. Electrochemical impedance spectroscopy (EIS) of the carbon fiber and CFO coated carbon fiber (a), and CV profiles of the S (b) and CFO coating (c).

paper and dried in air oven for 12 h at 60 °C, followed by being cut into circular electrodes with the sulfur loading of about 1.8 mg/cm<sup>2</sup>. The cathode disks and CFO interlayers with the diameter of 16 mm were dried in a vacuum oven for 12 h at 60 °C before assembling the cell. The electrolyte comprised 1.0 M lithium bis (trifluoromethanesulfonyl) imide (LiTFSI) and 5% LiNO<sub>3</sub> salts dissolved in dimethoxymethane (DME) and 1,3-dioxolane (DOL) (GuoTaiHuaRong Co., Ltd.) at a 1:1 volume ratio. The concentration of sulfur in the electrolyte was about 20 μL/mg. CR2030 coin cells were assembled with sulfur cathodes, electrolyte, CFO coated interlayers, polypropylene separators (Celgard) and lithium foils.

### 2.3. Assessment of the performances

The wettability of the samples was measured by OCA-20 type contact angle test platform (Germany). Chemistry of the samples was characterized by X-ray diffraction (XRD) (D8 Advance diffractometer, Bruker, Germany) operated using Cu K $\alpha$  radiation. XPS measurements were carried out on an Axis Ultra DLD X-ray photoelectron spectrometer using monochromatic Al K $\alpha$  (1486.6 eV) radiation. Morphology of the coatings was examined by scanning electron microscopy (SEM, JSM-7800F) equipped with EDX. Relatively long-term cycling stability, rate capacity and discharge/charge performances were evaluated

through a Neware Battery Measurement System with the voltage range of 3.0–1.8 V (Vs. Li<sup>+</sup>/Li). Electrochemical impedance spectroscopy (EIS) of the cells was recorded with a CHI660E electrochemical workstation (Shanghai ChenHua Co., Ltd.) over the frequency range of 100 kHz to 100 mHz.

### 3. Results and discussion

The CFO coatings were successfully deposited on carbon fiber (Fig. 1). It is noted that under photograph, the CFO coated interlayers are grey dark in color (Fig. 1a) as compared to the uncoated carbon fiber. Original carbon fiber paper showed hydrophobic feature with a contact angle of 140° (Fig. 1b), indicating its poor surface wettability. However, after the deposition of CFO coating, remarkably altered wettability was recognized for the carbon fiber paper with a sharply decreased water contact angle 17° (Fig. 1c). This high hydrophilicity is beneficial to attract the terminal sulfur of dissolved LPS. The coating exhibited excellent adsorption performances for LPS during the 12 h stewing (the inset photo in Fig. 1c). These properties were likely attributed to the synergistic roles played by carbon fiber and the CFO coating, which should not block charge transfer and the electrochemical redox reaction at the adsorption interface. SEM and EDS elements mapping patterns of the CFO coating suggest that the carbon

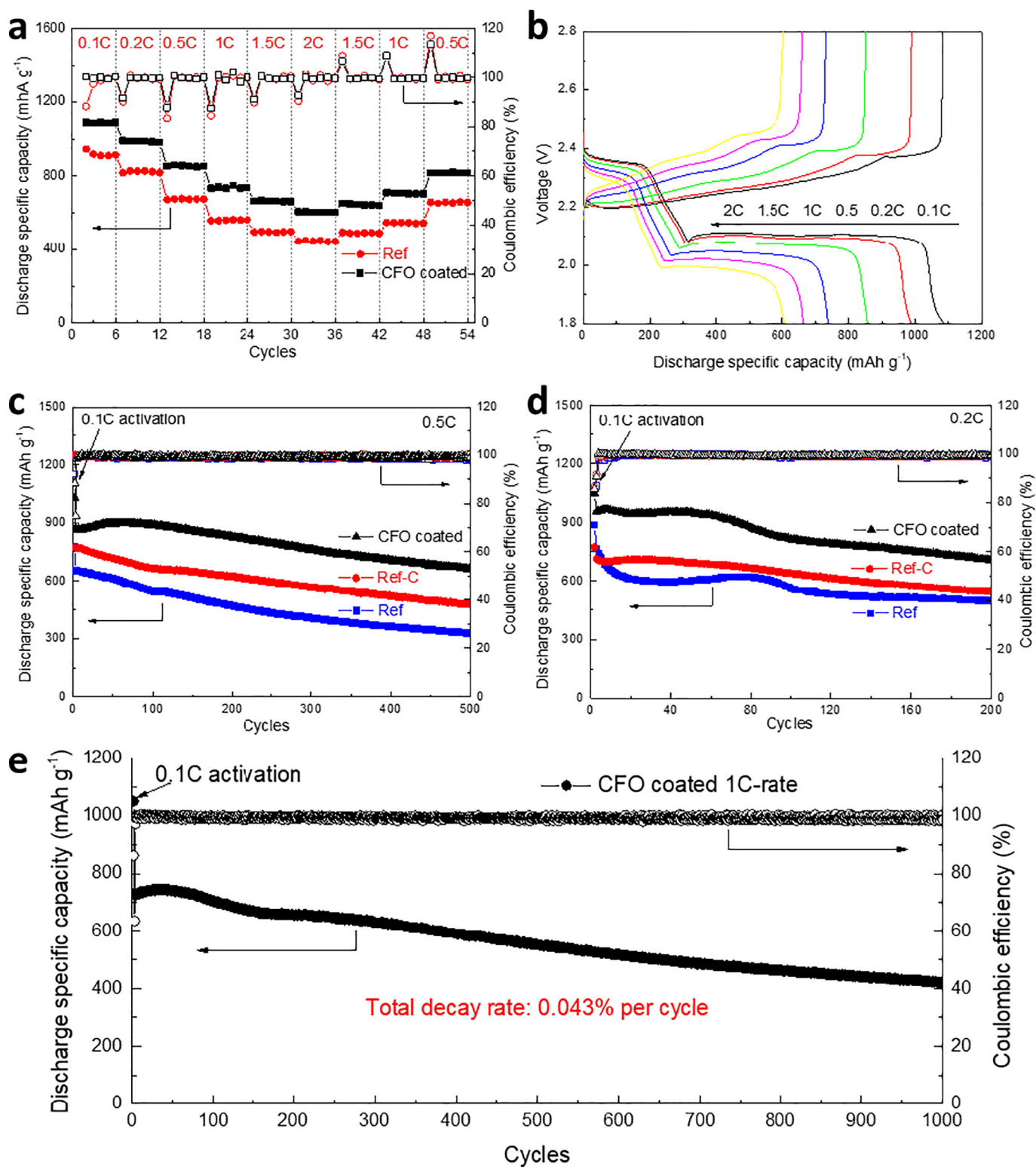


Fig. 4. (a) Rate performance of CFO coated interlayer and Reference, (b) Charge/discharge voltage profiles of CFO coated interlayer in rate test. (c) Cycling performances at current rate of 0.5C, and (d) 0.2C of the two interlayer. (e) Long-term cycling capacity and coulombic efficiency of CFO coated interlayer at 1C.

fiber substrate was completely enwrapped by the coating (Fig. 1d), the porous morphology and good electrical conductivity of the interlaced carbon fiber would facilitate penetration of electrolyte and fast electron/ion transport. The CFO coating showed uniformly small ripple-like surface features (Fig. 1e), which is inherited from the pyrolysis spraying processing. Further element analyses (the inset table in Fig. 1e) revealed the atom ratio of Co to Fe of ~1:2, which is consistent with the

original proportion of the precursors. The appearance of little Cl element is likely attributed to the remained chlorinated cobalt or hydrochloric acid used for cleaning the substrate before the spraying. Fortunately it seems that the presence of Cl did not affect the adsorption performance of the CFO coating. In addition, uniform distribution of the element C, Co, Fe, O in the selected areas was also realized (Fig. 1f-i), which further suggests unique coating deposition on carbon fiber.

XRD was used to confirm the structure of the prepared CFO coating (Fig. 2a). Compared to the carbon fiber substrate, a little peak [311] and [220] of the cubic  $\text{CoFe}_2\text{O}_4$  were emerge with a low intensity and broad width, that meant a low crystallinity of the CFO coating, showed an amorphous structure. XPS analysis was carried out to investigate the components and elemental valences of the CFO coating (Fig. 2b–f). Fig. 2b showed the wide scan survey spectra of CFO coating which presented Co2p, Fe2p, O1s and C1s. The XPS characteristic peaks of Co2p located at 780.7 eV and 796.0 eV respectively, and two shake-up satellite peaks at 784.4 eV and 804.1 eV dictated the strong presence of  $\text{Co}^{2+}$  (Fig. 2c). Fig. 2d showed the characteristic signals of Fe 2p at 711.4 eV and 724.9 eV which were due to Fe2p 3/2 and Fe2p1/2, at the position of 715.9 eV was a satellite peaks of the Fe2p. The results indicated the presence of  $\text{Fe}^{3+}$  and  $\text{Co}^{2+}$  in the coating. O1s spectra indicated three peaks at 530.1 eV, 531.6 eV and 533.6 eV denoted as lattice oxygen which was bound to metals, defects and the hydroxyl group present respectively (Fig. 2e). C1s spectra peak at 284.8 eV and 285.6 eV and 288.6 eV meant the C–C, C–H and C=O bond respectively in the carbon fiber (Fig. 2f).

Further electrochemical testing showed that the CFO coated and uncoated carbon fiber exhibited almost the same Ohm impedance values (Fig. 3a), indicating that the introduction of thin CFO layer did not trigger obvious changes in Ohm resistance of the cell. In this configuration cell, the CFO coated interlayer could work as an upper current collector for the S cathode, enhancing the active material utilization and thereby raising the specific capacity of the cell. The redox potential of the LPS lie in the range  $2.1 \text{ V} \leq E^{\circ} \leq 2.4 \text{ V}$  versus  $\text{Li}/\text{Li}^+$  (Fig. 3b), this is corresponding to the other works [2,41]. The CFO coated carbon fiber have a low redox potential (1.87 V) versus  $\text{Li}/\text{Li}^+$  (Fig. 3c), below the redox voltage of soluble LPS, according to the theory previous [2], CFO is redox inactive towards LPS, only to bind LPS via polar interaction.

To further clarify the blocking effect of the new interlayer on dissolved polysulfide, the performances of the assembled cells were evaluated (Fig. 4). The testing was carried out based on a coin cell configuration with no interlayer (labeled as Ref) and carbon fiber interlayer (Ref-C) as the reference samples. The discharge specific capacities and columbic efficiencies acquired under different current rates (Fig. 4a), it was noted that the average specific capacities of the CFO-coated interlayer reached 1086, 987, 855, 739, 664 and 604  $\text{mAh g}^{-1}$  at 0.1, 0.2, 0.5, 1.0, 1.5 and 2C, respectively under the sulfur loading of about  $1.8 \text{ mg cm}^{-2}$ . The high discharge capacity of 0.1C demonstrated the enhanced active material utilization by the CFO-coated carbon fiber interlayer. Moreover, the capacities of 645, 706 and 818  $\text{mAh g}^{-1}$  were recovered when the current density switched back to 1.5, 1.0 and 0.5C, a bit lower than those measured before the current switching, suggesting well reversible rate cycling performance.

Charge/discharge voltage profiles of the CFO-coated interlayer exhibited two discharge plateaus that were consistent with the cyclic voltammogram plots (Fig. 4b). The upper discharge plateau indicated the transformation of elemental sulfur to soluble long-chain LPS ions  $\text{S}_{n-2}$  ( $4 < n < 8$ ), and the lower discharge plateau suggested the transformation of long-chain LPS to short-chain LPS,  $\text{Li}_2\text{S}_2$  and  $\text{Li}_2\text{S}$ , which were also the inherent discharge platform curve of lithium-sulfur batteries [5,42].

The galvanostatic cycling testing was performed at 0.1C for activation followed by 0.5C and 0.2C, respectively (Fig. 4c–d). For the CFO-coated interlayer examined at 0.2C, an initial capacity of  $955 \text{ mAh g}^{-1}$  and a retained capacity of  $708 \text{ mAh g}^{-1}$  after 200 cycles were obtained, corresponding to the capacity retention of  $\sim 74\%$ . With the carbon fiber interlayer, the capacity retention was almost identical compared with the CFO-coated interlayer, presumably suggesting that the simply inserted physical barrier layer could improve the cycling stability of the cell. These results were in agreement with other published results [43,44]. However, the reference sample without the interlayer only delivered a capacity retention of 65%, which was lower than that of the

cell comprising the CFO-coated interlayer. During the 0.5C cycling, the CFO-coated interlayer showed an initial capacity of  $873 \text{ mAh g}^{-1}$  and the capacity retention of 76% after 500 cycles (Fig. 4d). While,  $478 \text{ mAh g}^{-1}$  and  $327 \text{ mAh g}^{-1}$  were maintained with a capacity retention of 62%, 50% after 500 cycles by the cell with the carbon fiber interlayer and no interlayer cell respectively. It nevertheless indicated that the presence of the CFO coating not only increased the specific capacities but also enhanced resistance of the capacity against decay. Therefore, long-term cycling of the cells containing the CFO-coated interlayer was assessed with 1C-rate at sulfur loading of  $1.72 \text{ mg cm}^{-2}$ . An initial peak capacity of  $733 \text{ mAh g}^{-1}$  and a capacity retention of 57% after 1000 cycles were realized (Fig. 4e). The calculated degradation ratio during the overall 1000 cycles was 0.043% per cycle. The charge efficiency of the first several cycles of 0.2C, 0.5C and 1C was higher than 100%, which could be explained by the re-utilization of the sulfur core in cathode. This outstanding cycling stability was regarded to be resulted from the chemical adsorption of the CFO coating. The wrapped corrugated coating would inhibit the dissolution of LPS in the electrolyte. Chemisorption enabled spatially located  $\text{Li}_2\text{S}$  precipitation on the surface of the CFO coating, in turn transferring the LPS to a host current collector of excellent conductive carbon fiber. This ultimately gives rise to significantly improved cell performances.

#### 4. Conclusions

$\text{CoFe}_2\text{O}_4$  coatings were deposited by spray pyrolysis technique on carbon fiber, which acted as the interlayer in Li-S batteries. The coating homogeneously wrapped the wall of the carbon fiber and excellent hydrophilic had been achieved. Significant spatial physical blocking and chemical adsorption of dissolved LPS in the assembled battery cell was realized, which prevented effectively the shuttling of the LPS. The confined LPS on the CFO coating surface together with the carbon fiber acted as a host current collector, which was reutilized in the charge/discharge process. These phenomena further improved effectively the utilization of the active materials and specific capacities of the cell. Significantly improved electrochemical performances, a remarkable low decay rate of 0.043% per cycle during 1000 cycles at 1C-rate under the sulfur loading of  $1.72 \text{ mg cm}^{-2}$  had been achieved. The results shed light on developing innovative fabrication method and research strategies using the binary metal oxide coating materials for next generation Li-S batteries.

#### Acknowledgements

This work is supported by National Natural Science Foundation of China through Grant No.51802322, Ningbo Natural Science Foundation Grant No.2018A610082 and Ningbo Key High-Tech R&D “2025” Program Grant No.20181ZDYF020113.

#### References

- [1] W.M. Kang, et al., A review of recent developments in rechargeable lithium-sulfur batteries, *Nanoscale* 8 (37) (2016) 16541–16588.
- [2] X. Liang, et al., Tuning transition metal oxide-sulfur interactions for long life lithium sulfur batteries: the “goldilocks” principle, *Adv. Energy Mater.* 6 (6) (2016).
- [3] J. Shim, K.A. Striebel, E.J. Cairns, The lithium/sulfur rechargeable cell - effects of electrode composition and solvent on cell performance, *J. Electrochem. Soc.* 149 (10) (2002) A1321–A1325.
- [4] S.E. Cheon, et al., Rechargeable lithium sulfur battery - I. Structural change of sulfur cathode during discharge and charge, *J. Electrochem. Soc.* 150 (6) (2003) A796–A799.
- [5] X.L. Ji, K.T. Lee, L.F. Nazar, A highly ordered nanostructured carbon-sulphur cathode for lithium-sulphur batteries, *Nat. Mater.* 8 (6) (2009) 500–506.
- [6] J.L. Wang, et al., Sulfur composite cathode materials for rechargeable lithium batteries, *Adv. Funct. Mater.* 13 (6) (2003) 487–492.
- [7] F. Wu, et al., A polypyrrole-supported carbon paper acting as a polysulfide trap for lithium-sulfur batteries, *RSC Adv.* 5 (114) (2015) 94479–94485.
- [8] Y.V. Mikhaylik, J.R. Akridge, Polysulfide shuttle study in the Li/S battery system, *J. Electrochem. Soc.* 151 (11) (2004) A1969–A1976.
- [9] X. Liu, et al., Nanostructured metal oxides and sulfides for lithium-sulfur batteries,

- Adv. Mater. 29 (20) (2017).
- [10] X.J. Zhu, et al., Electrochemical characterization and performance improvement of lithium/sulfur polymer batteries, *J. Power Sources* 139 (1–2) (2005) 269–273.
- [11] Y.J. Zhong, et al., Trapping sulfur in hierarchically porous, hollow indented carbon spheres: a high-performance cathode for lithium-sulfur batteries, *J. Mater. Chem. A* 4 (24) (2016) 9526–9535.
- [12] H.M. Yan, et al., Three-dimensional nitrogen-doped graphene/sulfur composite for lithium-sulfur battery, *Ionics* 22 (11) (2016) 1999–2006.
- [13] S.H. Chung, A. Manthiram, A hierarchical carbonized paper with controllable thickness as a modulable interlayer system for high performance Li-S batteries, *Chem. Commun.* 50 (32) (2014) 4184–4187.
- [14] Y.S. Su, A. Manthiram, Lithium-sulphur batteries with a microporous carbon paper as a bifunctional interlayer, *Nat. Commun.* 3 (2012).
- [15] L.Y. Zhang, et al., Preparation of a macroscopic, robust carbon-fiber monolith from filamentous fungi and its application in Li-S batteries, *Green Chem.* 16 (8) (2014) 3926–3934.
- [16] L.Y. Chai, et al., Porous carbonized graphene-embedded fungus film as an interlayer for superior Li-S batteries, *Nano Energy* 17 (2015) 224–232.
- [17] C.J. Hart, et al., Rational design of sulphur host materials for Li-S batteries: correlating lithium polysulphide adsorptivity and self-discharge capacity loss, *Chem. Commun.* 51 (12) (2015) 2308–2311.
- [18] Z.W. Seh, et al., Sulphur-TiO<sub>2</sub> yolk-shell nanoarchitecture with internal void space for long-cycle lithium-sulphur batteries, *Nat. Commun.* 4 (2013).
- [19] J. Liu, et al., SnO<sub>2</sub> as a high-efficiency polysulfide trap in lithium-sulfur batteries, *Nanoscale* 8 (28) (2016) 13638–13645.
- [20] J. Zhang, et al., High performance of electrochemical lithium storage batteries: ZnO-based nanomaterials for lithium-ion and lithium-sulfur batteries, *Nanoscale* 8 (44) (2016) 18578–18595.
- [21] X. Liang, et al., A highly efficient polysulfide mediator for lithium-sulfur batteries, *Nat. Commun.* 6 (2015).
- [22] L. Kong, Y. Handa, I. Taniguchi, Synthesis and characterization of sulfur-carbon-vanadium pentoxide composites for improved electrochemical properties of lithium-sulfur batteries, *Mater. Res. Bull.* 73 (2016) 164–170.
- [23] H. Tang, et al., In-situ synthesis of carbon@Ti<sub>4</sub>O<sub>7</sub> non-woven fabric as a multi-functional interlayer for excellent lithium-sulfur battery, *Electrochim. Acta* 263 (2018) 158–167.
- [24] Y.R. Zhong, et al., Mechanistic insights into surface chemical interactions between lithium polysulfides and transition metal oxides, *J. Phys. Chem. C* 121 (26) (2017) 14222–14227.
- [25] Z. Li, et al., A sulfur host based on titanium monoxide@carbon hollow spheres for advanced lithium-sulfur batteries, *Nat. Commun.* 7 (2016).
- [26] J.R. He, et al., Yolk-shelled C@Fe<sub>3</sub>O<sub>4</sub> nanoboxes as efficient sulfur hosts for high-performance lithium-sulfur batteries, *Adv. Mater.* 29 (34) (2017).
- [27] Z.G. Yin, et al., Rationally designed hollow precursor-derived Zn<sub>3</sub>V<sub>2</sub>O<sub>8</sub> nanocages as a high-performance anode material for lithium-ion batteries, *Nano Energy* 31 (2017) 367–376.
- [28] Y.Q. Chu, Z.W. Fu, Q.Z. Qin, Cobalt ferrite thin films as anode material for lithium ion batteries, *Electrochim. Acta* 49 (27) (2004) 4915–4921.
- [29] Y.N. NuLi, Q.Z. Qin, Nanocrystalline transition metal ferrite thin films prepared by an electrochemical route for Li-ion batteries, *J. Power Sources* 142 (1–2) (2005) 292–297.
- [30] X.H. Yang, W. Xiong, Z. Zhang, Electrochemical properties of submicron cobalt ferrite spinel through a co-precipitation method, *J. Cryst. Growth* 277 (1–4) (2005) 467–470.
- [31] M. Bahat, et al., Synthesis, characterization and magnetic properties of micro-crystalline lithium cobalt ferrite from spent lithium-ion batteries, *J. Mater. Process. Technol.* 183 (1) (2007) 117–121.
- [32] S.S. Bellad, C.H. Bhosale, Substrate temperature dependent properties of sprayed CoFe<sub>2</sub>O<sub>4</sub> ferrite thin films, *Thin Solid Films* 322 (1–2) (1998) 93–97.
- [33] A.K. Bhosale, et al., Spray deposited CeO<sub>2</sub>-TiO<sub>2</sub> counter electrode for electrochromic devices, *Bull. Mater. Sci.* 38 (2) (2015) 483–491.
- [34] K.F. Azizi, M.M. Bagheri-Mohagheghi, The effect of solution flow rate and substrate temperature on structural and optical properties of TiO<sub>2</sub> films deposited by spray pyrolysis technique, *Thin Solid Films* 621 (2017) 98–101.
- [35] Z.K. Heiba, et al., Effect of vanadium doping on structural and magnetic properties of defective nano-nickel ferrite, *Appl. Phys. Mater. Sci. Process.* 124 (4) (2018).
- [36] A. Mouden, et al., Synthesis and characterization of CuO thin films grown by chemical spray pyrolysis, *Opt. Quant. Electron.* 49 (2) (2017).
- [37] B. Yuliarto, et al., Preparation of SnO<sub>2</sub> thin film nanostructure for CO gas sensor using ultrasonic spray pyrolysis and chemical bath deposition technique, *Acta Phys. Pol. A* 131 (3) (2017) 534–538.
- [38] A. Arfaoui, et al., Physical and ethanol sensing properties of sprayed Fe<sub>2</sub>(MoO<sub>4</sub>)<sub>3</sub> thin films, *J. Alloys Compd.* 719 (2017) 392–400.
- [39] S.S. Kumbhar, et al., Fabrication of ZnFe<sub>2</sub>O<sub>4</sub> films and its application in photo-electrocatalytic degradation of salicylic acid, *J. Photochem. Photobiol. B Biol.* 142 (2015) 118–123.
- [40] N. Karthigayan, et al., Synthesis and characterization of NiFe<sub>2</sub>O<sub>4</sub>, CoFe<sub>2</sub>O<sub>4</sub> and CuFe<sub>2</sub>O<sub>4</sub> thin films for anode material in Li-ion batteries, *Nanomater. Nanotechnol.* 7 (2017).
- [41] M. Cuisinier, et al., Sulfur speciation in Li-S batteries determined by operando X-ray absorption spectroscopy, *J. Phys. Chem. Lett.* 4 (19) (2013) 3227–3232.
- [42] X.Y. Tao, et al., Balancing surface adsorption and diffusion of lithium-polysulfides on nonconductive oxides for lithium-sulfur battery design, *Nat. Commun.* 7 (2016).
- [43] Y.S. Su, A. Manthiram, A new approach to improve cycle performance of rechargeable lithium-sulfur batteries by inserting a free-standing MWCNT interlayer, *Chem. Commun.* 48 (70) (2012) 8817–8819.
- [44] C.X. Zu, et al., Improved lithium-sulfur cells with a treated carbon paper interlayer, *Phys. Chem. Chem. Phys.* 15 (7) (2013) 2291–2297.